ISSN 0915-633X

NATIONAL INSTITUTE FOR FUSION SCIENCE

Some Problems inside a Mass Analyzer for Pions Extracted from a H_2 Gas Discharge

J. Uramoto

(Received - Feb. 10, 1998)

NIFS-543 Mar. 1998

RESEARCH REPORT
NIFS Series

NAGOYA, JAPAN

Some problems inside a mass analyzer for pions extracted from a H_2 gas discharge

Jōshin URAMOTO

National Institute for Fusion Science,

Oroshi-cho, Toki-shi, Gifu, 509-5292, Japan

Abstract

When positive or negative pions are extracted with (H^+, H_2^+, H_3^+) ions or H^- ions and enter a magnetic mass analyzer MA of 90° deflection type, some problems occur, which are very different from mass analyses of classical charged particles. Because the pions can penetrate indirectly metal plates (which include a beam collector itself of MA) while μ-neutrino ν_μ and anti-μ-neutrino $\bar{\nu}_\mu$ beams generate. This phenomenon becomes serious when (H^+, H_2^+, H_3^+) ions or H^- ions are reflected by a back metal lid plate of MA and are supplied around the beam collector.

Keywords: pion, μ-neutrino, back metal plate, positive ion

1. Introduction

We have reported[1),2)] already that positive or negative pions and muons are extracted from outside of a H_2 gas discharge along magnetic field, and that μ-neutrino ν_μ and anti-μ-neutrino $\bar{\nu}_\mu$ beams are produced secondarily. These ν_μ and $\bar{\nu}_\mu$ neutrinos penetrate metal plates MP easily and generate negative or positive muons in the opposite side of MP if positive ions or electrons are supplied in the opposite side. Thus, many problems occur in mass analyses by an ordinary mass analyzer when the pions and muons are extracted with H^- ions or H^+, H_3^+ ions. In this paper, these problems will be shown under a magnetic mass analyzer of 90° deflection-type.

2. Detections of H^-, π^-, μ^-

Schematic diagrams of the experimental apparatus are shown in Figs. 1. The apparatus is constructed from a H_2 gas discharge plasma in magnetic fields, three extraction electrodes (with an aperture of 3 mm in diameter) to extract some negatively charged particles and a magnetic mass analyzer (90° deflection-type).

A sheet plasma[3)] is produced to generate H^- ions effectively and in wide area. That is, the discharge (cylindrical) plasma flow of about 1 cm in diameter is transformed into a sheet plasma flow of about 3 mm in thickness and about 20 cm in width. The sheet plasma flow enters the anode through the main chamber (50 cm long). A uniform magnetic field of about 50 gauss is applied along the sheet plasma flow in the main chamber where the H_2 gas pressure is about 1.5×10^{-3} Torr. The anode current I_A is 20A. A distance between the sheet plasma center and the first extraction electrode (L) is 7.5 cm. The plasma density in the center of the sheet plasma is about 10^{11}/cc and the electron temperature is about 20 eV. The positive ion density in front of the first extraction electrode is estimated to be about 10^{10}/cc from a positive ion saturation current as H_3^+, while the electron density from the Langmuir probe characteristic is about 10^9/cc and the electron temperature is about 3.0 eV. That is, the electron density in front of the first extraction electrode is reduced near 1/10 of the positive ion density.

The negatively charged particles extracted from the H_2 gas discharge plasma, are injected into the ordinary magnetic mass analyzer (MA) through the slit (3 mm × 1 cm) while each mass of the negatively charged particle is estimated by the following relations: From the analyzing magnetic

field B_M where the negative current to the beam collector BC shows a peak, the curvature radius r of the mass analyzer and the extraction (acceleration) voltage V_E, we can estimate the mass m of the negatively charged particle by,

$$m = \frac{Ze\,(B_M r)^2}{2V_E}$$

$$= \frac{8.8 \times 10^{-2}\, Z\,(B_M r)^2\, m_e}{V_E}, \quad \cdots\cdots (1)$$

where e is the electron charge, B_M is in gauss unit, r is in cm unit, V_E is in volt unit and m_e is the electron mass and Z is the charge number. For the curvature radius $r = 4.3$ cm of this mass analyzer, the Eq. (1) is rewritten by

$$m = \frac{1.63\, Z\, B_M^2}{V_E} m_e. \quad \cdots\cdots (2)$$

In the extraction of negatively charged particles, the first extraction electrode (L) is electrically floated, whose potential V_L is about -10V with respect to the anode (11). A potential V_M of the second extraction electrode (M) is kept at 100V. A potential V_E of the final extraction electrode (E) is 800V.

In this experiment, it is noted that the back space of the beam collector is shielded[4] perfectly from the diffusion of positive ions as shown in Fig. 1 (B). The dependences of the negative current I^- to the beam collector on the analyzing magnetic field B_M are shown in Fig. 2 for the beam collector potential $V_{BC} = 0$V and $V_{BC} = 100$V. Obviously, in a case (1) of Fig. 2, a main peak of I^- at the analyzing magnetic field $B_M \approx (4.0 \times 240)$ gauss = 960 gauss is corresponding to H^- ion, assuming that $Z = 1$ in Eq. (2). That is, we obtain $m \approx 1880\ m_e$ (near the true mass of H^- = 1842 m_e) as $V_E = 800$V. Then, we find that the middle peak of I^- at $B_M \approx (1.54 \times 240)$ gauss $\approx$ 370 gauss is corresponding to a negative pion, assuming that $Z = 1$ in Eq. (2). That is, we obtain $m \approx 278\ m_e$ (near the true pion mass = 273 m_e) as $V_E = 800$V.

Similarly, we find that the first peak of I^- at $B_M \approx (1.33 \times 240)$ gauss = 320 gauss is corresponding to a negative muon, assuming that $Z = 1$ in Eq. (2). That is, we obtain $m = 209\ m_e$ (near the true muon mass = 207 m_e) as $V_E = 800$V.

When a positive potential $V_{BC} = 100V$ is applied to the beam collector BC, their peaks of I^- increase, as seen in a case (2), about 1.3 times for H^- ion, about 300 times of π^- or μ^-. These large apparent increments of negative current peaks under the positive bias potential $V_{BC} > 0$ of the beam collector BC, can be explained from assistance of positive ions in front of BC[5].

3. Detections of H^+ (H_3^+), π^+, μ^+

Schematic diagrams of the experimental apparatus are shown in Figs. 3. The apparatus is constructed from the same H_2 gas discharge plasma with the case of H^-, π^-, μ^- in Figs. 1, three extraction electrodes to extract some "positively" charged particles and the mass analyzer where the polarity of analyzing magnetic field B_M is reversed (to $-B_M$).

The positively charged particles extracted from the H_2 gas discharge plasma, are injected into the magnetic mass analyzer (MA) while each mass of the positively charged particles is estimated by the same relations of Eq. (1) and Eq. (2) with the case of H^-, π^-, μ^-. In the extraction of positively charged particles, the first extraction electrode (L) is electrically floated, whose potential V_L is about $-10V$ with respect to the discharge anode. A potential V_M of the second extraction electrode (M) is $-100V$ and a potential V_E of the final extraction electrode (E) in $-800V$.

The dependences of the positive current I^+ to BC on $(-B_M)$ are shown in Fig. 4 for the beam collector potential $V_{BC} = 0V$. Obviously, in Fig. 4, a large peak of I^+ at $-B_M \approx (4.0 \times 240)$ gauss $=$ 960 gauss is corresponding to H^+ ion, assuming that $Z = 1$ in Eq. (2). That is, we obtain $m \approx 1880\ m_e$ as $|V_E| = 800V$. Another large peak of I^+ at $-B_M \approx (6.8 \times 240)$ gauss $\approx$ 1630 gauss is corresponding to H_3^+ ion, assuming that $Z = 1$ in Eq. (2). That is, we obtain $m \approx 5420\ m_e$.

Next, two small peaks of I^+ to BC are seen in Fig. 4. We find that the first peak at $-B_M \approx (1.35 \times 240)$ gauss $\approx$ 324 gauss is corresponding to a positive muon (μ^+) and the second peak at $-B_M \approx (1.60 \times 240)$ gauss $\approx$ 384 gauss is corresponding to a positive pion (π^+), assuming that $Z =$ 1 in Eq. (2). That is, we obtain $m \approx 210\ m_e$ (near the true muon mass 207 m_e) for the first peak and $m \approx 300\ m_e$ (near the true pion mass 273 m_e) for the second peak.

In these detections of the positively charged particles, even if the bias potential V_{BC} of BC is varied from 100V to $-100V$, the peak currents of I^+ are not varied. That is, no apparent current increments are observed in comparison with the cases of the negatively charged particles.

Thus, we conclude that a pair creation of π^- (μ^-) and π^+ (μ^+) particle is arised outside of the H_2 gas discharge plasma in magnetic fields and that the π^- and μ^- particles are detected easily as the apparent current to BC of MA increases extremely when positive bias voltage is applied to BC and positive ions are supplied in front of BC through reflection of H^- ions as shown in Fig. 1 (B).

4. Problems of mass analyzer for π^- and π^+

When negative pion π^- beam or positive pion π^+ beam is shot into a thick metal plate MP, the π^- or π^+ beam generates a μ-neutrino ν_μ beam or an anti-μ-neutrino $\bar{\nu}_\mu$ beam which penetrates MP easily. Then, if the positive ions (above a critical energy) are supplied behind MP, a negative muon μ^- beam appears continuously behind MP. Thus, some problems occur when negative pions π^- or positive ions π^+ are extracted with H^- ions or H^+ (H_3^+) ions from outside of the H_2 gas discharge and are analyzed by the magnetic mass analyzer of 90° deflection type. The insides of the mass analyzer and the magnetic field distribution are shown in Figs. 5 where the back metal plate BMP reflects H^- ions (as H^+ ions) and the insulator Ins interrupts the diffusion of H^+ ions behind the beam collector BC. Dependences of the beam collector current I^- on the analysis magnetic field B_M are shown in Fig. 2 when the BMP and the Ins exist inside the mass analyzer MA.

In the first stage of the following experiments for extraction of negatively charged particles, the BMP is removed as shown in Fig. 6 (A) from the MA while dependences of the negative current I^- are shown in Fig. 6 (B). We find that an apparent increment of the I^- of π^- or μ^- due to the positive beam collector bias voltage V_{BC} disappears and a net current of the I^- of π^- or μ^- appears independently of V_{BC}.

In the second stage, the Ins is removed as shown in Fig. 7 (A) while dependences of the I^- are shown in Fig. 7 (B). We find that both the apparent increment of the I^- of π^- or μ^- and the net current of the I^- of π^- or μ^- disappear even if the beam collector bias voltage V_{BC} is given.

In the third stage, both the BMP and the Ins are removed as shown in Fig. 8 (A) while dependences of the I^- are shown in Fig. 8 (B). We find that the apparent increment of the I^- of π^- or μ^- disappears and only the net current of the I^- of π^- or μ^- appears.

From the above experimental stages, we can consider that the I^- of π^- or μ^- disappears when

the positive ions H^+ (from H^- ions) reflected by the BMP diffuse behind the beam collector BC, and that the π^- or μ^- seems to penetrate the BC indirectly in the case of Fig. 7.

For extraction of positively charged articles (π^+, μ^+, H^+ and H_3^+), a dependence of the positive current I^+ on the reversed analysis magnetic field ($-B_M$) are shown already in Fig. 4 when the BMP and the Ins exist inside the MA. Similarly with the cases of negative particles, the I^+ current peak of π^+ or μ^+ disappears when only the Ins behind the BC is removed as shown in Fig. 9 (A). That is, the I^+ peak of π^+ or μ^+ appear when the BMP and the Ins exist or when both the BMP and the Ins are removed. Thus, we can consider also that the π^+ or μ^+ seems to penetrate the BC indirectly when the positive ions H^+, H_3^+ reflected by the BMP diffuse behind the BC.

5. Metal plate (MP) penetration of $\pi^\pm$ inside MA

(1) penetration of negative pion π^-

A potential V_M of the second extraction electrode (M) as shown in Fig. 1 (A) is varied at 300V from 100V while only the I^- current peak of π^- and the I^- current peak of H^- appear as shown in Fig. 10 (B). For a case without the metal plate MP inside MA as shown in Fig. 10 (A), a dependence of the I^- current on B_M is shown in Fig. 10 (B) under $V_{BC} = 0$ (where the BMP and the Ins exist).

In the first experiment of metal plate penetration of π^- inside MA, a thick (1 mm) metal plate MP is put as shown in Figs. 11 (A) and (B) where a distance between MP and BC is 2.0 cm. Then, a dependences of the negative current I^- on B_M is shown in Fig. 11 (C). A current peak of I^- appear between π^- peak and μ^- peak for the analyzing magnetic field B_M. In the second experiment, the BMP which reflects H^- ions (as H^+), is removed as shown in Fig. 12 (A) while the I^- current peak between π^- and μ^- as shown in Fig. 11 (C) disappears.

(2) Penetration of positive pion π^+

A potential V_M of the second extraction electrode (M) as shown in Fig. 3 (A) is varied at -300V from -100V while only the I^+ current peak of π^+ and the I^+ current peaks of H^+ and H_3^+ ions appear. For a case without the MP inside MA as shown in Fig. 13 (A), a dependence of the I^+ current on ($-B_M$) is shown in Fig. 13 (B).

In the first experiment of metal plate penetration of π^+ inside MA, a thick (1 mm) metal plate

MP is put as shown in Figs. 14 (A) and (B) where a distance between MP and BC is 2.0 cm. Then, the positive current I^+ corresponding to the π^+ beam does not appear while a negative current I^- corresponding to a negative muon μ^- beam appears as shown in Figs. 14 (A) and (B). This fact is estimated from about twice increment of the analyzing magnetic field ($-B_M$) in comparison with the case of negative pion π^- in Figs. 11 (A) and (B). Here, if the BMP which reflects H^+ and H_3^+ ions is removed as shown in Fig. 15, the I^- current peak of μ^- disappears.

As various references for the ($\pi^+ \rightarrow \mu^-$) transformation, the third experiment of $\overline{MP\text{–}BC}$ = 1.0 cm is shown in Figs. 16 (A) and (B), the forth experiment of $\overline{MP\text{–}BC}$ = 3.0 cm is shown in Fig. 17 where the I^- current peak of μ^- disappear, and the fifth experiment of $\overline{MP - BC}$ = 1.2 – 2.0 cm and (the thickness of MP) = 8 mm is shown in Figs. 18 (A) and (B).

These phenomena of metal plate penetration for π^- or π^+ can be explained only by the μ -neutrino ν_μ, the anti-μ-neutrino $\bar{\nu}_\mu$ and the positive ion effects behind the metal plate MP as reported[1),2)] already.

References

1) J. Uramoto: Research Report, NIFS–541 (1998).

2) J. Uramoto: Research Report, NIFS–542 (1998).

3) J. Uramoto: Journal of the vacuum society of Japan, **31** (1994) 507 in Japanese.

4) J. Uramoto: National Institute for Fusion Science, Oroshi-cho, Toki-shi, Gifu, 509-5292, Japan – Research Report, NIFS–400 (1996).

5) J. Uramoto: NIFS–512 (1997).

Figure Captions

Fig. 1 (A) Schematic diagram of experimental apparatus for negative particle detection under H_2 gas discharge.

1: Cylindrical plasma in discharge anode. 2: Discharge cathode. 3: H_2 gas flow. 4: Discharge power supply. 5: Electron acceleration power supply. 6: Vacuum pump. 7: Area where cylindrical plasma is transformed into sheet plasma. 8: Insulation tube. 9: A pair of permanent magnets. 10: Magnetic field coils. 11: Anode. I_A: Current to anode. CP: Cylindrical plasma. SP: Sheet plasma. B_Z: Magnetic field. L: First extraction electrode. M: Second extraction electrode. E: Final extraction electrode. V_M: Potential (100V) of second extraction electrode with respect to anode. V_E: Potential (800V) of final extraction electrode with respect to anode. MA: Magnetic deflection (90°) mass analyzer. B_M: Magnetic field intensity of MA. BC: Beam collector of MA. V_{BC}: Positive potential of BC with respect to MA. I^-: Negative current to BC. H_0^-: Hydrogen negative ions outside of sheet plasma. H^-: Accelerated hydrogen negative ions. π_0^-: Negative pion particles outside of sheet plasma. π^-: Accelerated negative pion particles.

Fig. 1 (B) Schematic diagram of mass analyzer for negative particle detection.

S: Entrance slit position. X: Entrance of uniform magnetic field.

Ins: Insulator behind BC. +Ion: Positive ions in front of BC. Fe: shows Iron.

Fig. 2 (1) Dependences of negative current I^- to BC on magnetic field B_M of MA under (1) beam collector potential $V_{BC} = 0V$ and (2) $V_{BC} = 100V$.

H^-: Peak of I^- corresponding to H^- ion. π^-: Peak of I^- corresponding to negative pion particle. μ^-: Peak of I^- corresponding to negative muon particle.

Fig. 3 (A) Schematic diagram of experimental apparatus for positive particle detection under H_2 gas discharge.

V_M: –100V. V_E: –800V. I^+: Positive current to BC. H_0^+: Hydrogen positive ions outside of sheet plasma. H^+: Accelerated hydrogen positive ions. π_0^+: Positive pion particles outside of sheet plasma. π^+: Accelerated pion particles.

(See captions of Fig. 1).

Fig. 3 (B) Schematic diagram of mass analyzer for positive particle detection.

$-B_M$: Reversed magnetic field of MA.

Fig. 4 Dependences of positive current I^+ to BC on reversed magnetic field ($-B_M$) of MA under beam collector bias voltage $V_{BC} = 0 \sim \pm 100V$.

π^+: Peak of I^+ corresponding to positive pion particle. μ^+: Peak of I^+ corresponding to positive muonlike particle. H^+ or H_3^+: Peak of I^+ corresponding to H^+ or H_3^+ ion.

Figs. 5 (A) and (B) Insides of the mass analyzer.

BMP: Back metal plate. H^+: Reflected hydrogen positive ions (from H^- ions). Ins: Insulator behind the beam collector BC. C: Magnetic coil. S: Entrance slit (3 mm × 10 mm). (N): North pole of electro-magnet. (S): South pole.

(See Captions of Figs. 1)

Fig. 5 (C) Fringe magnetic field distribution at 1A of MA coil current.

B_M: Analyzing magnetic field of MA. B_O: Uniform magnetic field inside MA. S: Entrance slit position. X: Entrance of uniform magnetic field.

Fig. 6 (A) Inside of MA without back metal plate BMP.

Fig. 6 (B) Dependences of the negative current I^- on the analyzing magnetic field B_M.

(1): Beam collector potential $V_{BC} = 0V$. (2): $V_{BC} = 100V$. H^-: Hydrogen negative ions. π^-: Negative pion. μ^-: Negative muon. V_E: 800V. $V_M = 100V$.

(See Captions of Figs. 1)

Fig. 7 (A) Inside of MA without Ins behind BC.

Fig. 7 (B) Dependences of the beam collector current I^- on B_M.

(1): $V_{BC} = 0V$. (2): $V_{BC} = 100V$.

Fig. 8 (A) Inside of MA without BMP and Ins.

Fig. 8 (B) Dependences of the beam collector current I^- on B_M.

(1): $V_{BC} = 0V$. (2) $V_{BC} = 100V$.

Fig. 9 (A) Dependence of the beam current (positive) I^+ on the reversed analysis magnetic field ($-B_M$) in a case without only Ins.

H^+ and H_3^+: Positive hydrogen ions.

Fig. 9 (B) Dependence of the I^+ on $(-B_M)$ in cases with both BMP and Ins or without both BMP and Ins.

π^+: Positive pions. μ^+: Positive muons.

Fig. 10 (A) Inside of MA for π^- and H^- without metal plate MP.

BMP: Back metal plate.

Fig. 10 (B) Dependences of the beam collector current I^- on B_M.

π^-: Negative pions. H^-: Negative hydrogen ions.

Figs. 11 (A) and (B) Inside of MA for π^- and H^- with metal plate MP.

$\overline{MP-BC}$ = 2.0 cm.

Fig. 11 (C) Dependence of the negative current I^- on B_M under MP.

Fig. 12 Inside of MA with MP and without BMP.

*No current peaks of the I^- appear.

Fig. 13 (A) Inside of MA for π^+ and H^+, H_3^+ without MP.

BMP: Back metal plate. π^+: Positive pions. H^+, H_3^+: Positive hydrogen ions.

Fig. 13 (B) Dependence of the positive beam collector current I^+ on the reversed analysis magnetic field $(-B_M)$.

*V_E = –800V. V_M = –300V.

(See Captions of Figs. 3).

Fig. 14 (A) Inside of MA with metal plate MP.

$\overline{MP-BC}$ = 2.0 cm. π^+: Positive pions. μ^-: Negative muons estimated from mass analysis.

Fig. 14 (B) Dependence of the negative beam collector current I^- on $(-B_M)$.

Fig. 15 Inside of MA without BMP and with MP.

*No current peaks appear.

Fig. 16 (A) Inside of MA with MP is a case of $\overline{MP-BC}$ = 1.0 cm.

μ^-: Negative muons.

Fig. 16 (B) Dependence of the negative beam collector current I^- on $(-B_M)$.

μ^-: Negative muons.

Fig. 17 Inside of MA with MP in a case of $\overline{MP - BC} = 3.0$ cm.

*No current peaks appear.

Fig. 18 (A) Inside of MA with a very thick (8 mm) metal plate MP.

$\overline{MP - BC} = 1.2 - 2.0$ cm.

Fig. 18 (B) Dependence of the negative beam collector current I^- on $(-B_M)$.

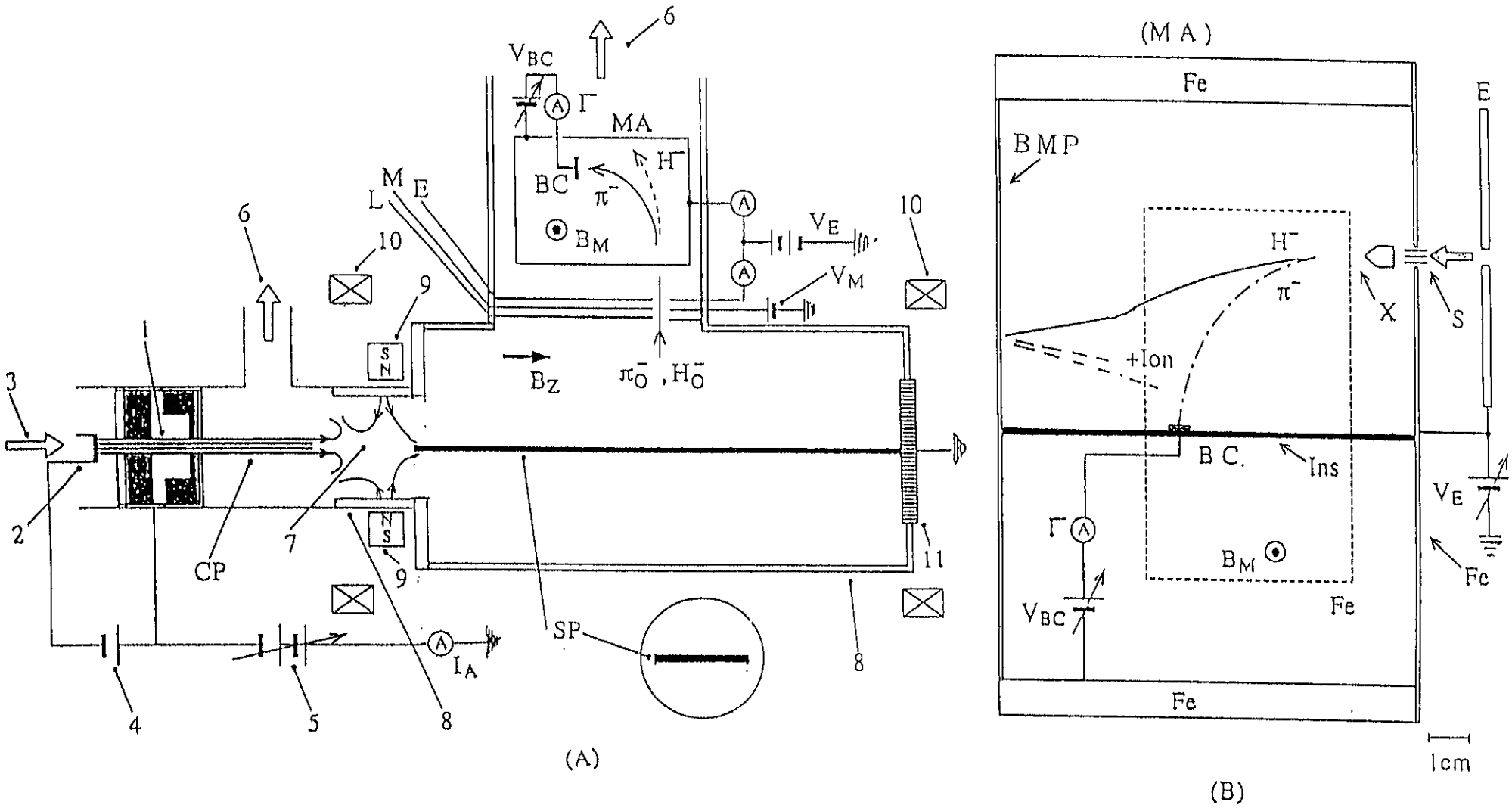
6
V_{BC}
Γ
MA
H⁻
BC
π⁻
B_M
M
L
E
V_E
V_M
10
9
S
N
B_Z
π_0^- , H_0^-
3
1
2
CP
7
11
SP
8
I_A
4
5
(A)
(M A)
Fe
BMP
E
+Ion
X
S
B C.
Ins
Fe
Fe
1cm
(B)

Fig. 1

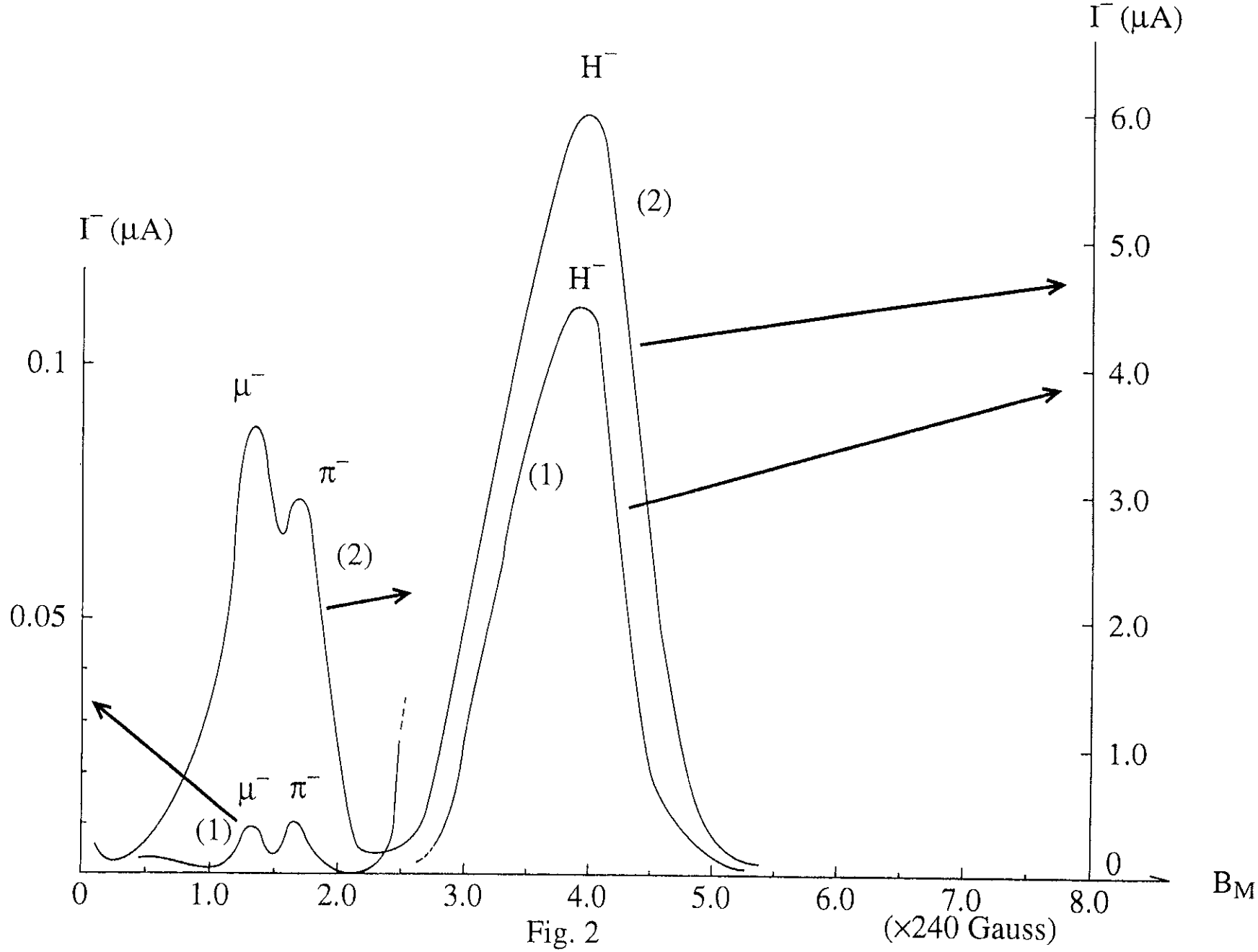
I⁻ (μA)
H⁻
(2)
H⁻
(1)
μ⁻
π⁻
(2)
μ⁻ π⁻
(1)
0.1
0.05
6.0
5.0
4.0
3.0
2.0
1.0
0
0 1.0 2.0 3.0 4.0 5.0 6.0 7.0 8.0
(×240 Gauss)
B_M

Fig. 2

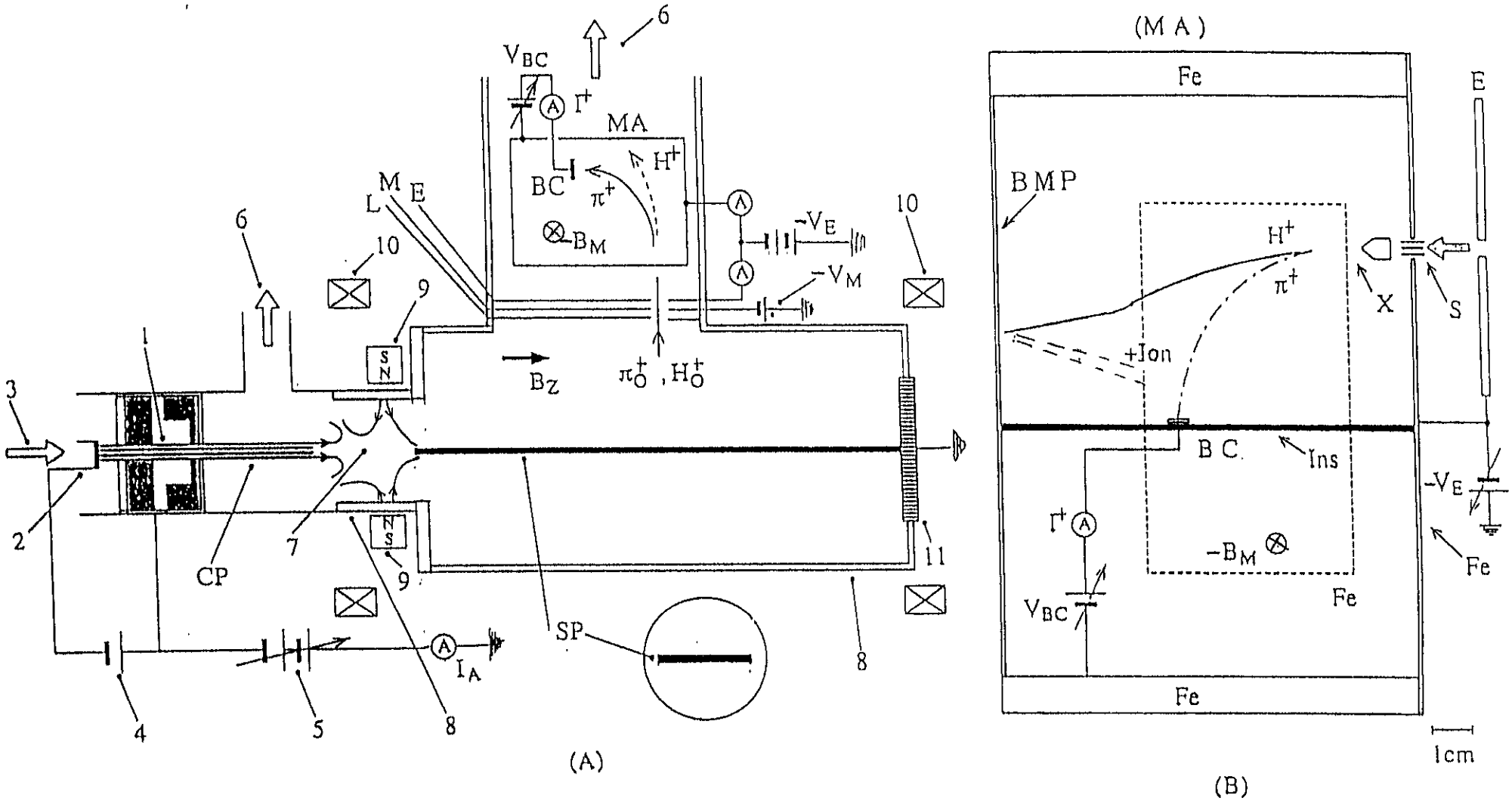
6
V_{BC}
I^+
MA
H^+
BC
π^+
B_M
M
L
E
$-V_E$
$-V_M$
10
9
B_Z
π_O^+ , H_O^+
3
1
2
CP
7
11
SP
8
4
5
I_A
(A)
(M A)
Fe
BMP
E
H^+
π^+
X
S
+Ion
B C
Ins
$-V_E$
I^+
$-B_M$
V_{BC}
Fe
1cm
(B)

Fig. 3

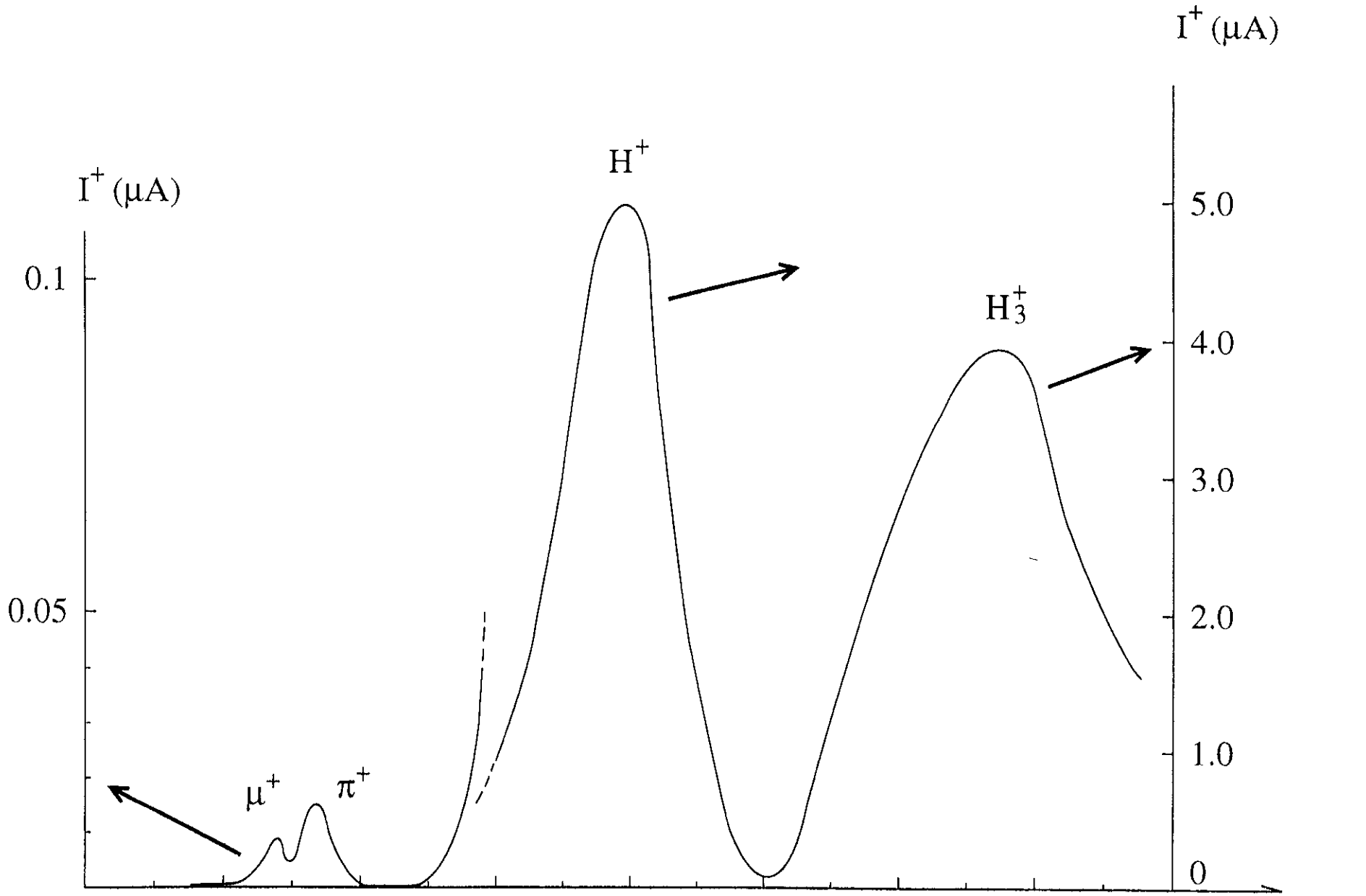
I+ (μA)
0.1
0.05
H+
H3+
μ+
π+
I+ (μA)
5.0
4.0
3.0
2.0
1.0
0
0
1.0
2.0
3.0
4.0
5.0
6.0
7.0
8.0
−BM
(×240 Gauss)

Fig. 4

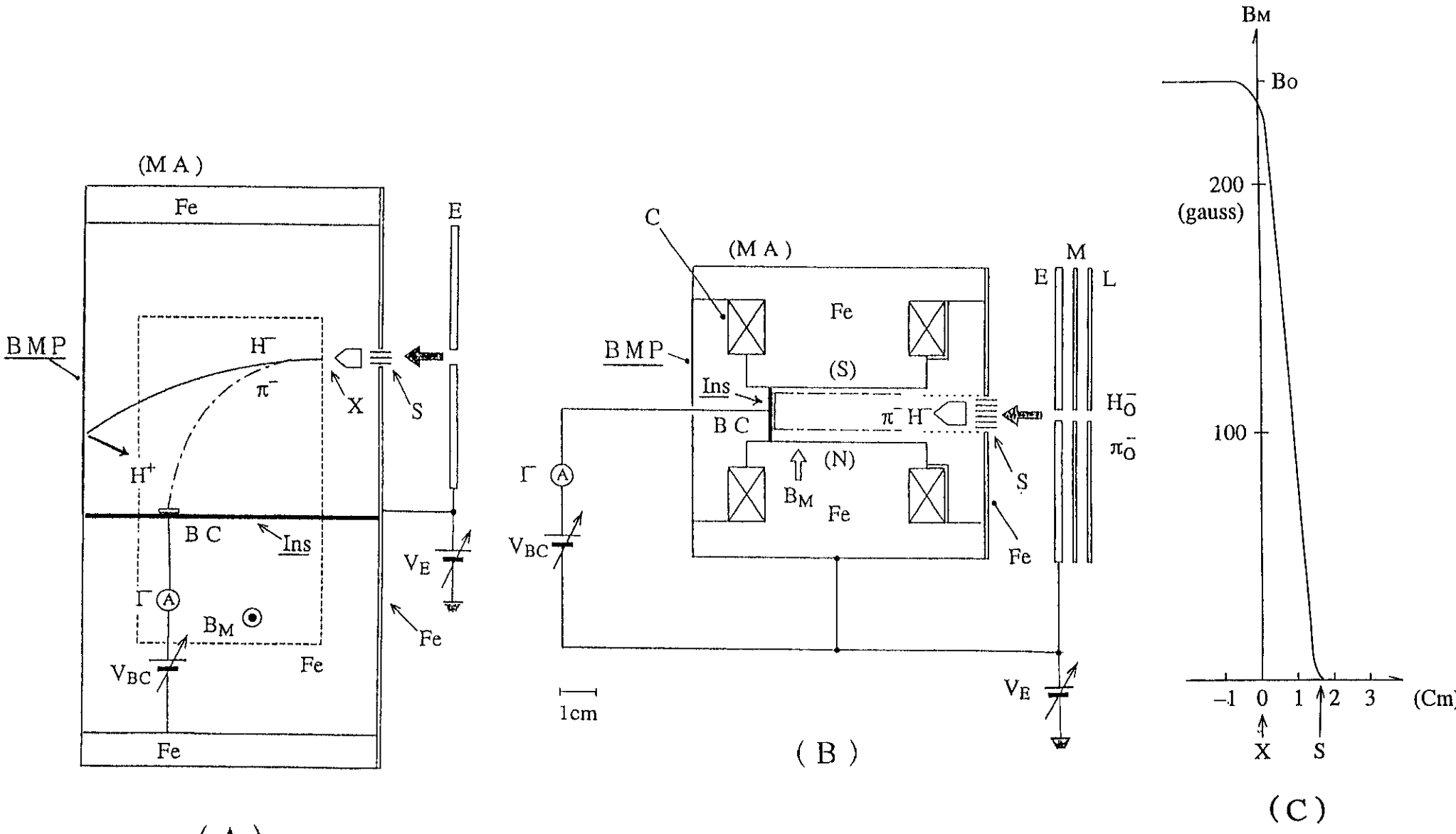
(M A)
Fe
E
BMP
H⁻
π⁻
X
S
H⁺
B C
Ins
Γ
A
VBC
BM
Fe
VE
Fe
Fe
(A)
C
(M A)
M
E
L
Fe
BMP
(S)
Ins
B C
π⁻ H⁻
H⁻O
π⁻O
(N)
BM
Fe
S
Γ
A
VBC
Fe
1cm
VE
(B)
BM
Bo
200
(gauss)
100
–1
0
1
2
3
(Cm)
X
S
(C)

Fig. 5

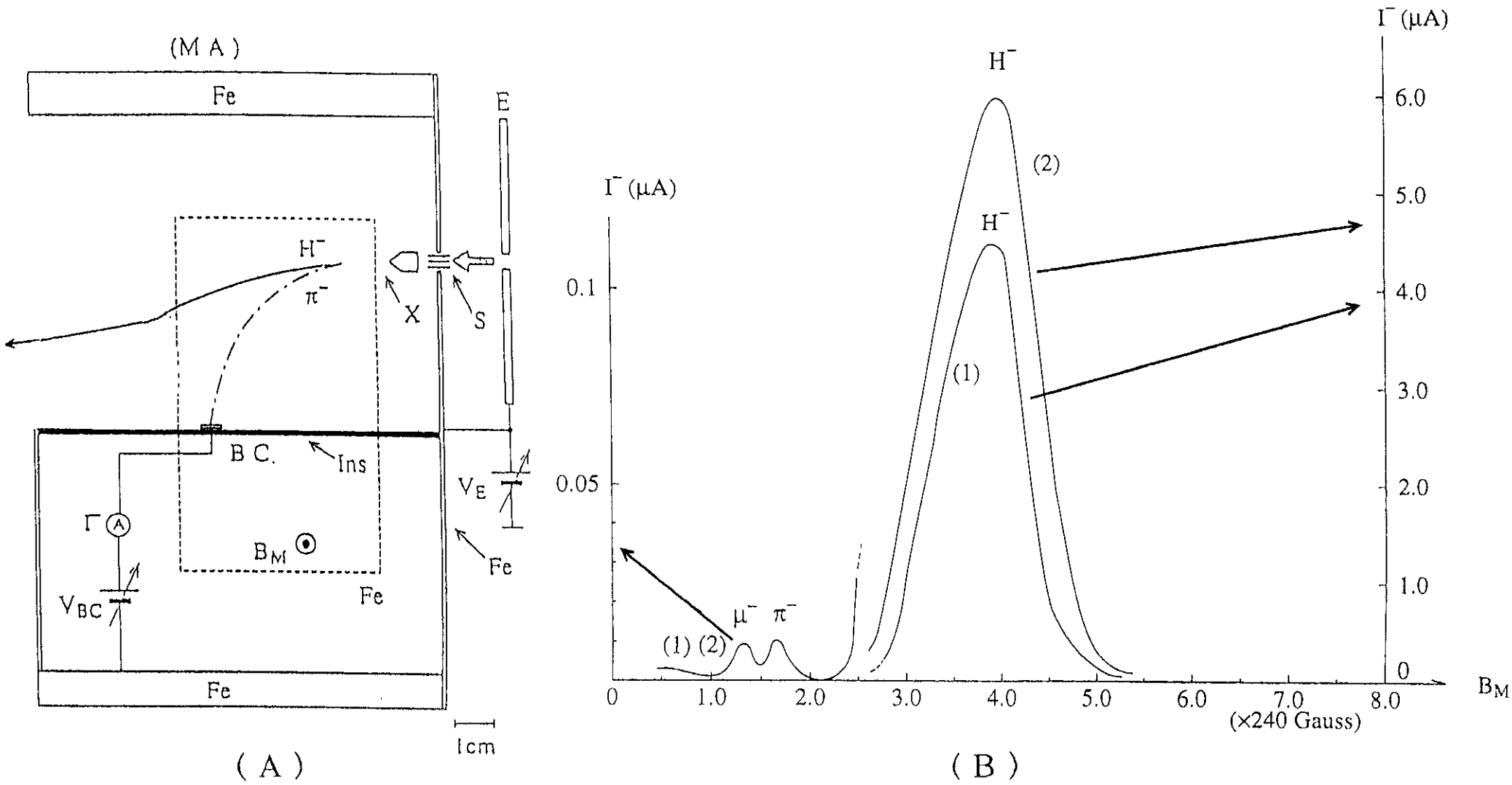
(M A)
Fe
E
H⁻
π⁻
X
S
B C.
Ins
Γ
A
B_M
V_BC
V_E
Fe
Fe
Fe
1cm
(A)
I⁻ (μA)
H⁻
(2)
H⁻
(1)
0.1
0.05
μ⁻ π⁻
(1) (2)
0
1.0
2.0
3.0
4.0
5.0
6.0
7.0
8.0
(×240 Gauss)
B_M
I⁻ (μA)
6.0
5.0
4.0
3.0
2.0
1.0
0
(B)

Fig. 6

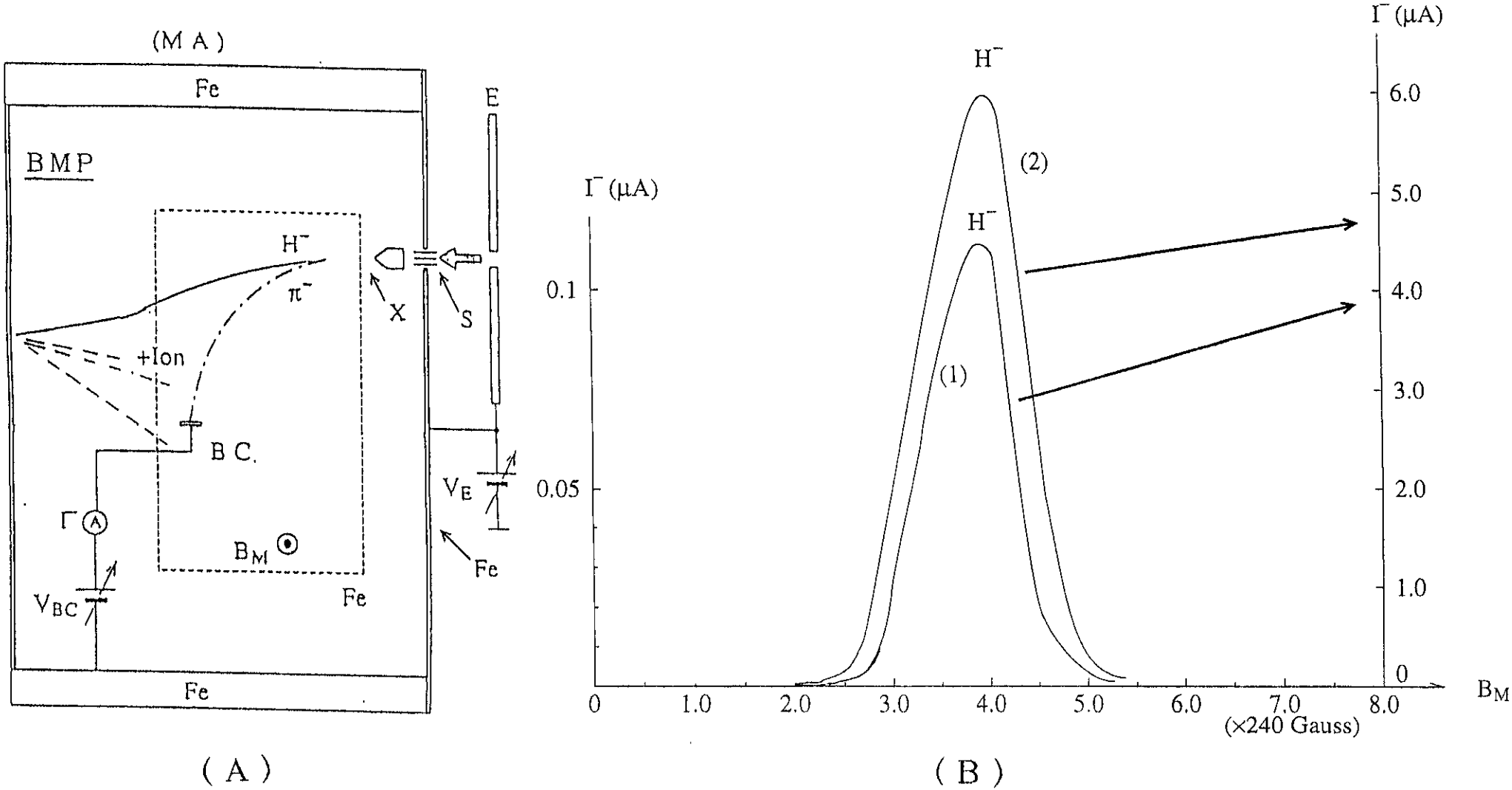
(M A)
Fe
BMP
E
H⁻
π⁻
X
S
+Ion
B C.
Γ
A
V_{BC}
B_M
Fe
V_E
Fe
Fe
(A)
I⁻ (μA)
0.1
0.05
H⁻
(2)
H⁻
(1)
I⁻ (μA)
6.0
5.0
4.0
3.0
2.0
1.0
0
0
1.0
2.0
3.0
4.0
5.0
6.0
7.0
8.0
(×240 Gauss)
B_M
(B)

Fig. 7

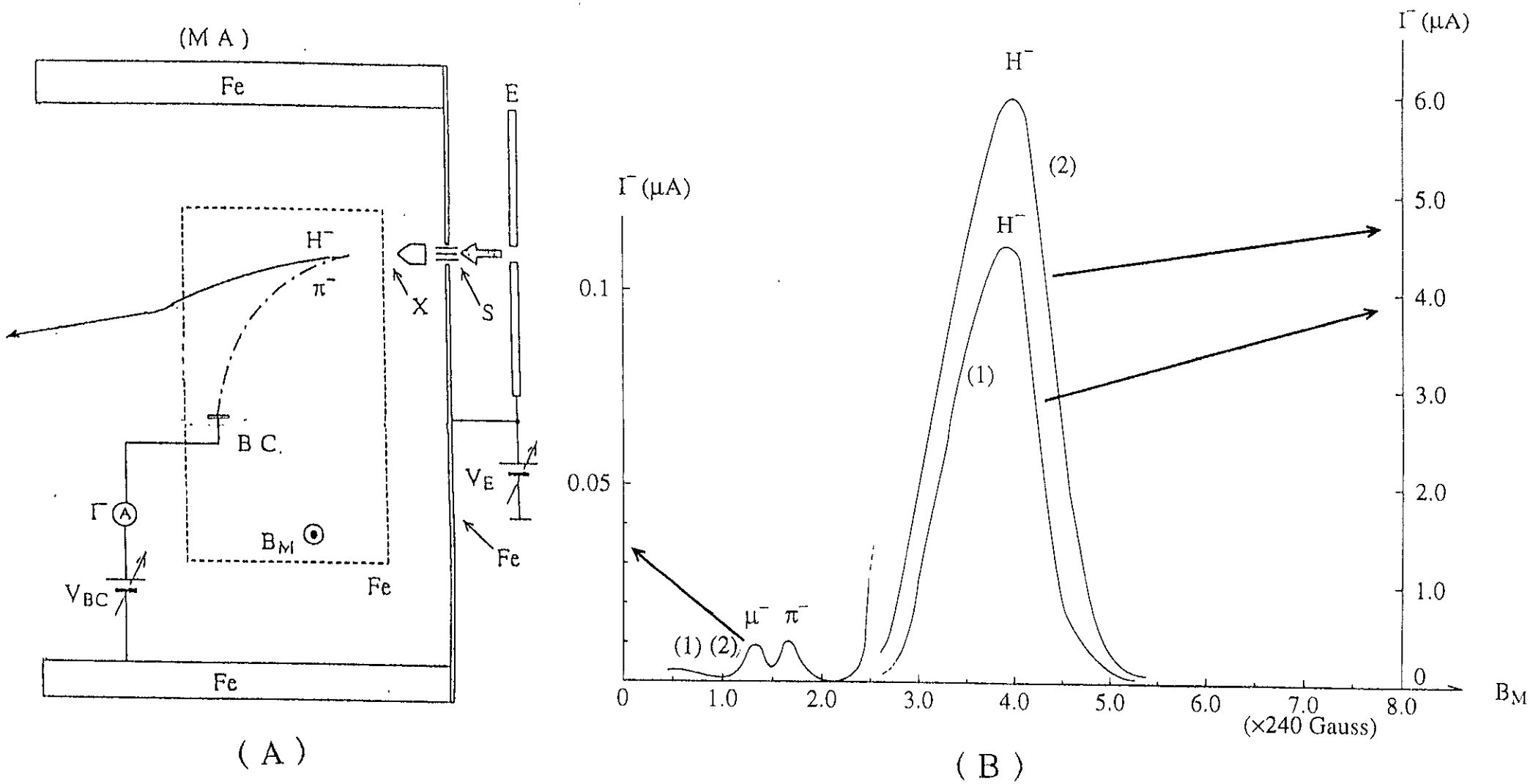
(M A)
Fe
E
H⁻
π⁻
X
S
B C.
Γ
A
B_M
V_BC
V_E
Fe
Fe
Fe
(A)
Γ⁻ (μA)
0.1
0.05
H⁻
(2)
H⁻
(1)
μ⁻ π⁻
(1) (2)
0
1.0
2.0
3.0
4.0
5.0
6.0
7.0
8.0
(×240 Gauss)
B_M
Γ⁻ (μA)
6.0
5.0
4.0
3.0
2.0
1.0
0
(B)

Fig. 8

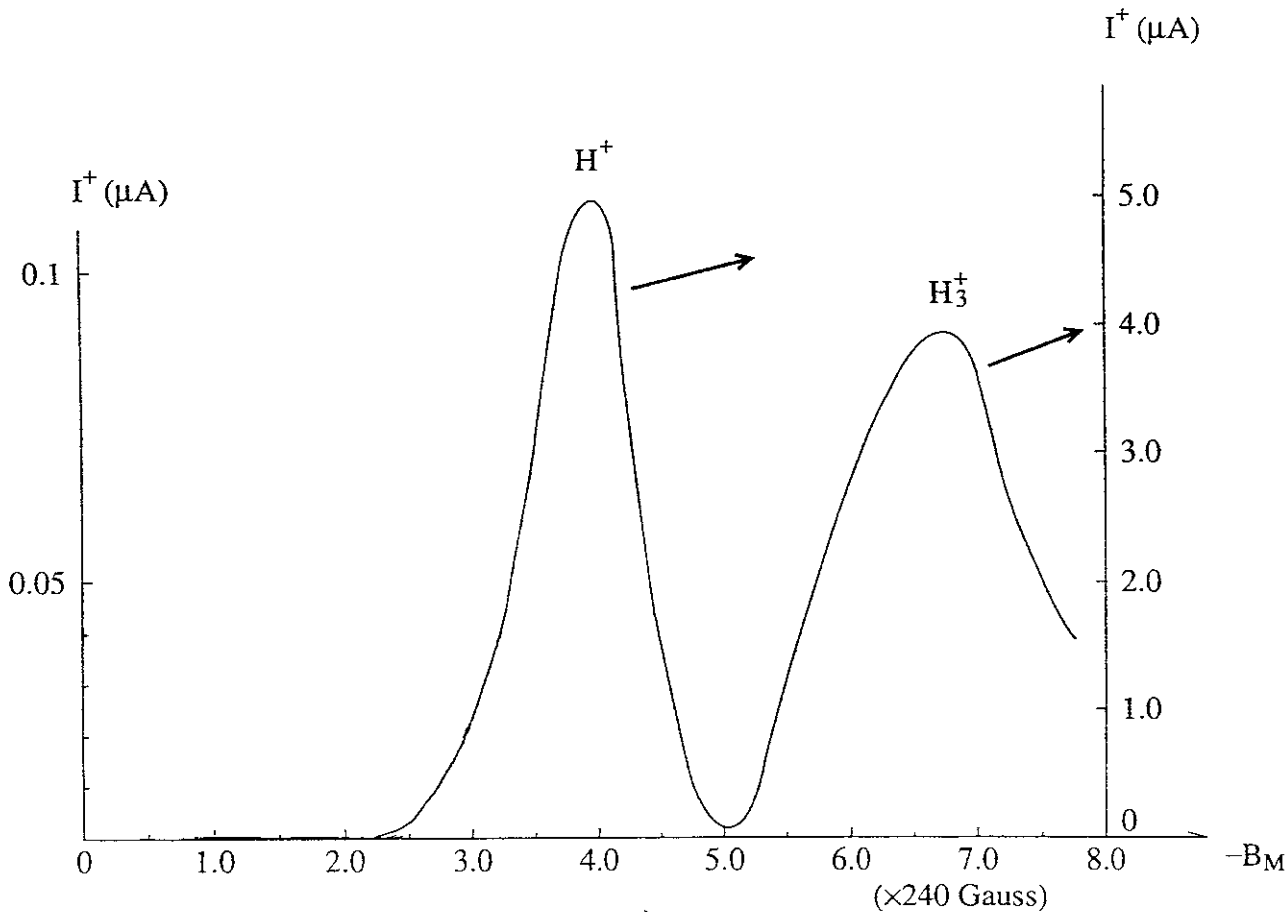
I+ (μA)
H+
H3+
0.1
0.05
5.0
4.0
3.0
2.0
1.0
0
0
1.0
2.0
3.0
4.0
5.0
6.0
7.0
8.0
−BM
(×240 Gauss)

(A)

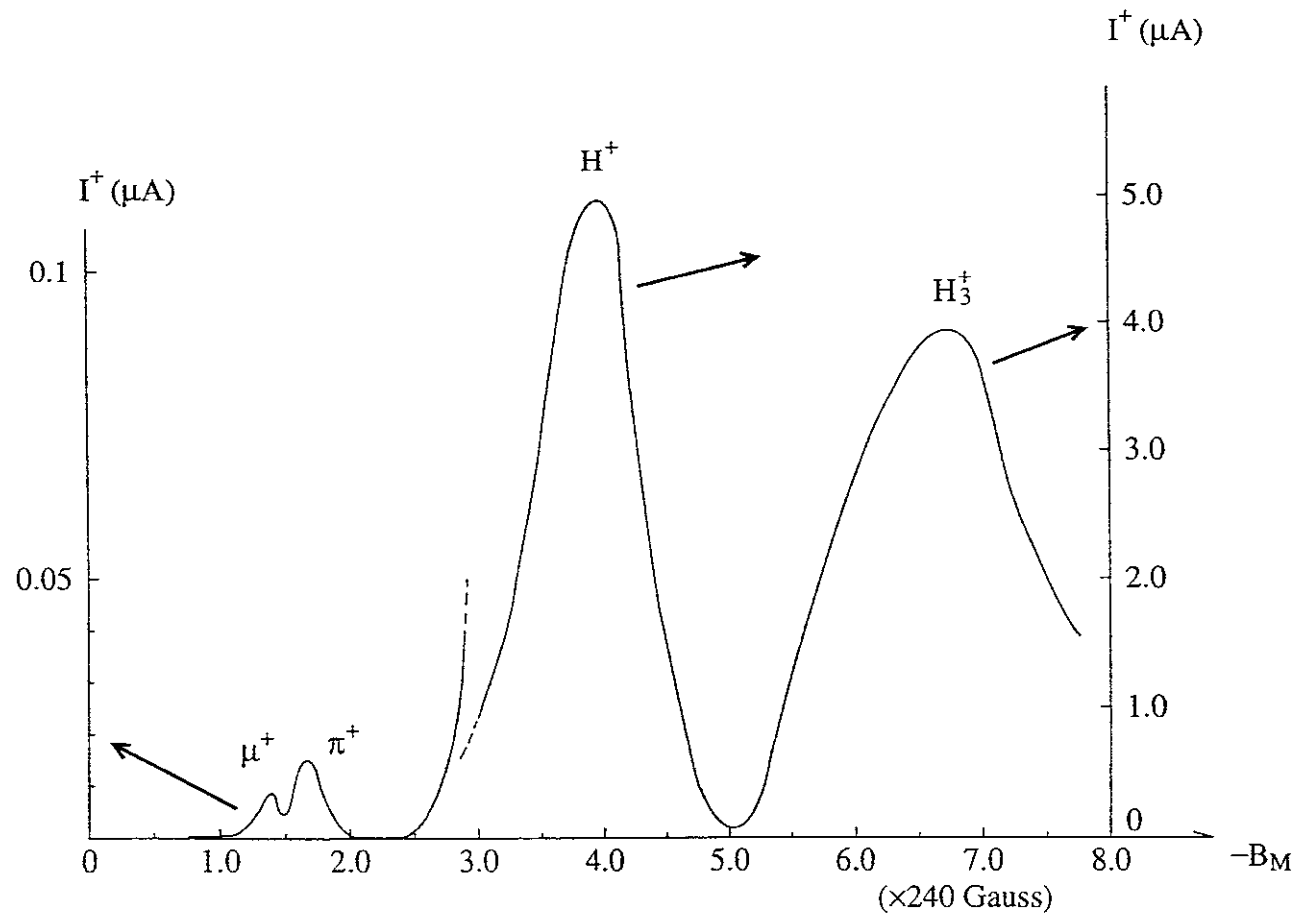
I+ (μA)
H+
H3+
0.1
0.05
5.0
4.0
3.0
2.0
1.0
0
μ+
π+
0
1.0
2.0
3.0
4.0
5.0
6.0
7.0
8.0
−BM
(×240 Gauss)

(B)

Fig. 9

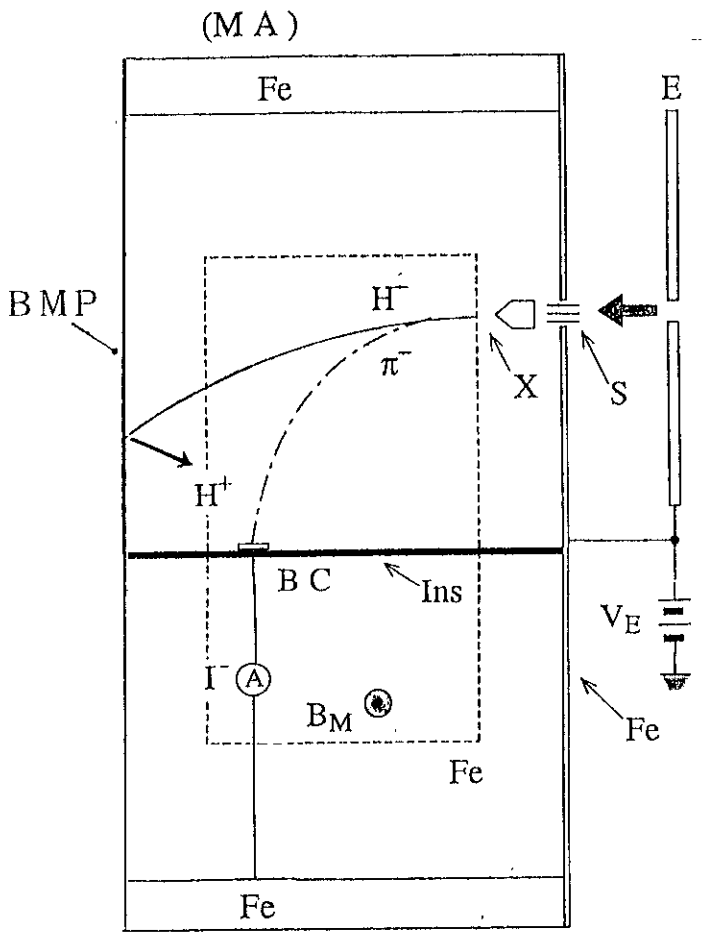

Fig. 10 (A)

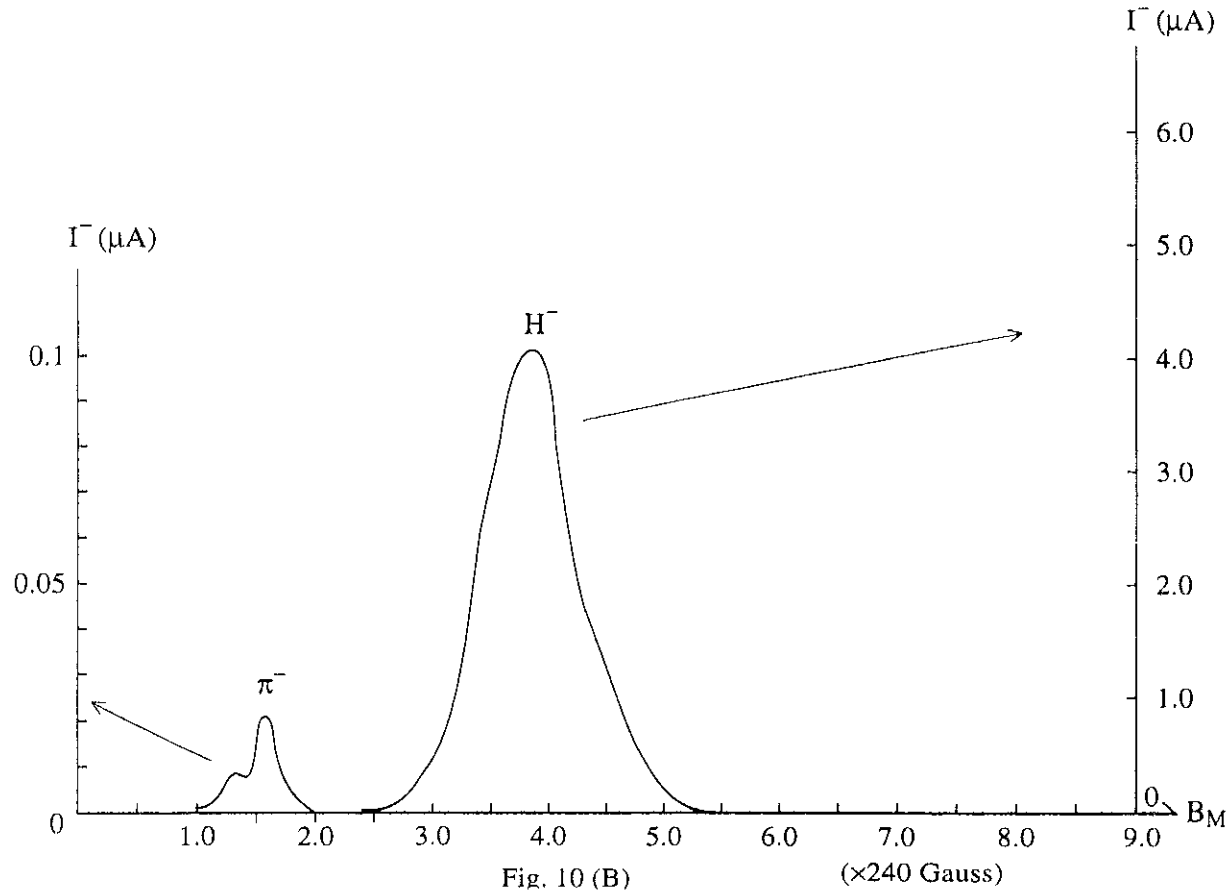

Fig. 10 (B)

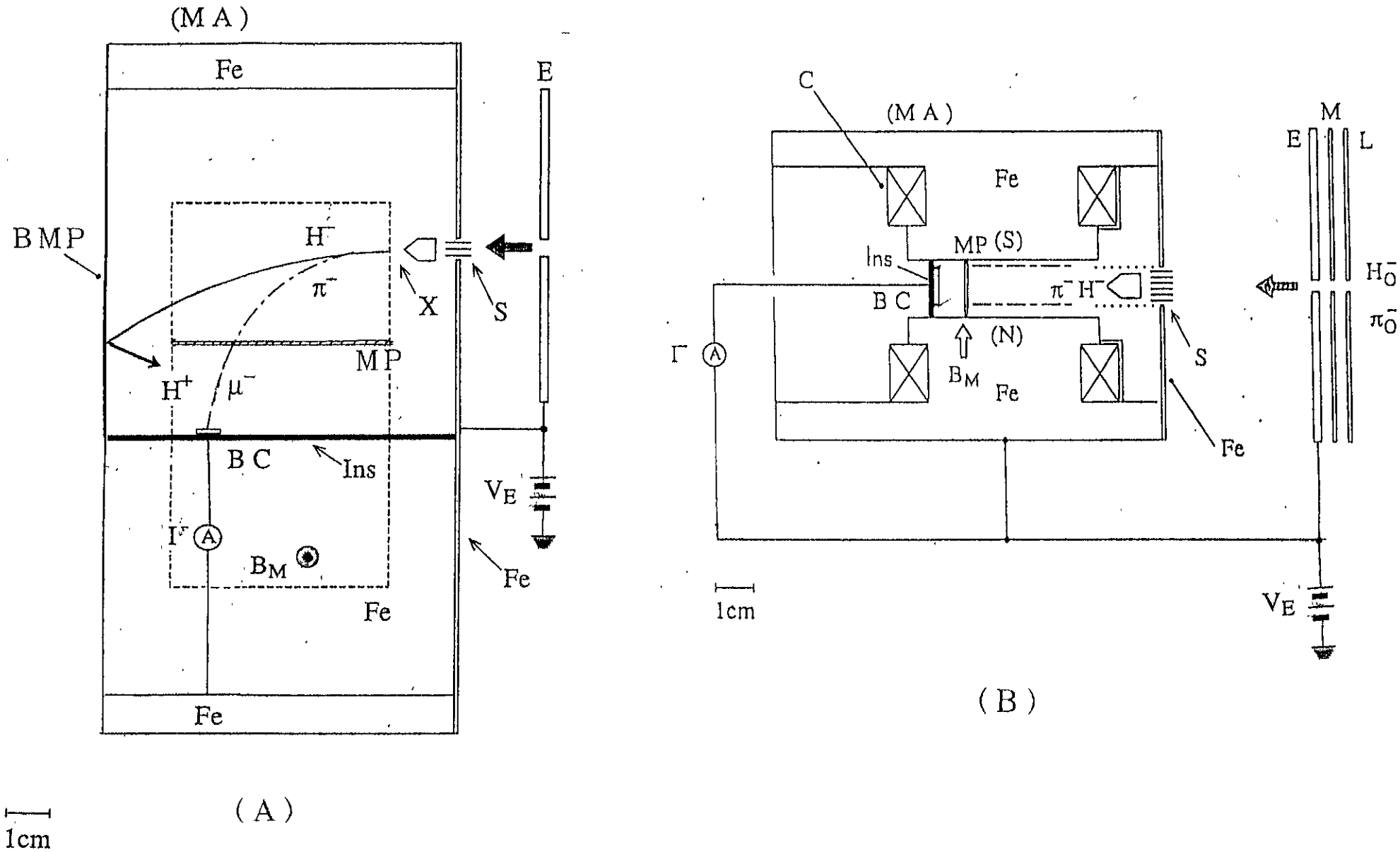
(M A)
Fe
E
BMP
H⁻
π⁻
X
S
MP
H⁺
μ⁻
BC
Ins
VE
I⁻
A
BM
Fe
Fe
Fe
1cm
(A)
C
(M A)
Fe
M
E
L
MP (S)
Ins
BC
π⁻ H⁻
H⁻O
π⁻O
(N)
S
Γ
A
BM
Fe
Fe
1cm
VE
(B)

Fig. 11

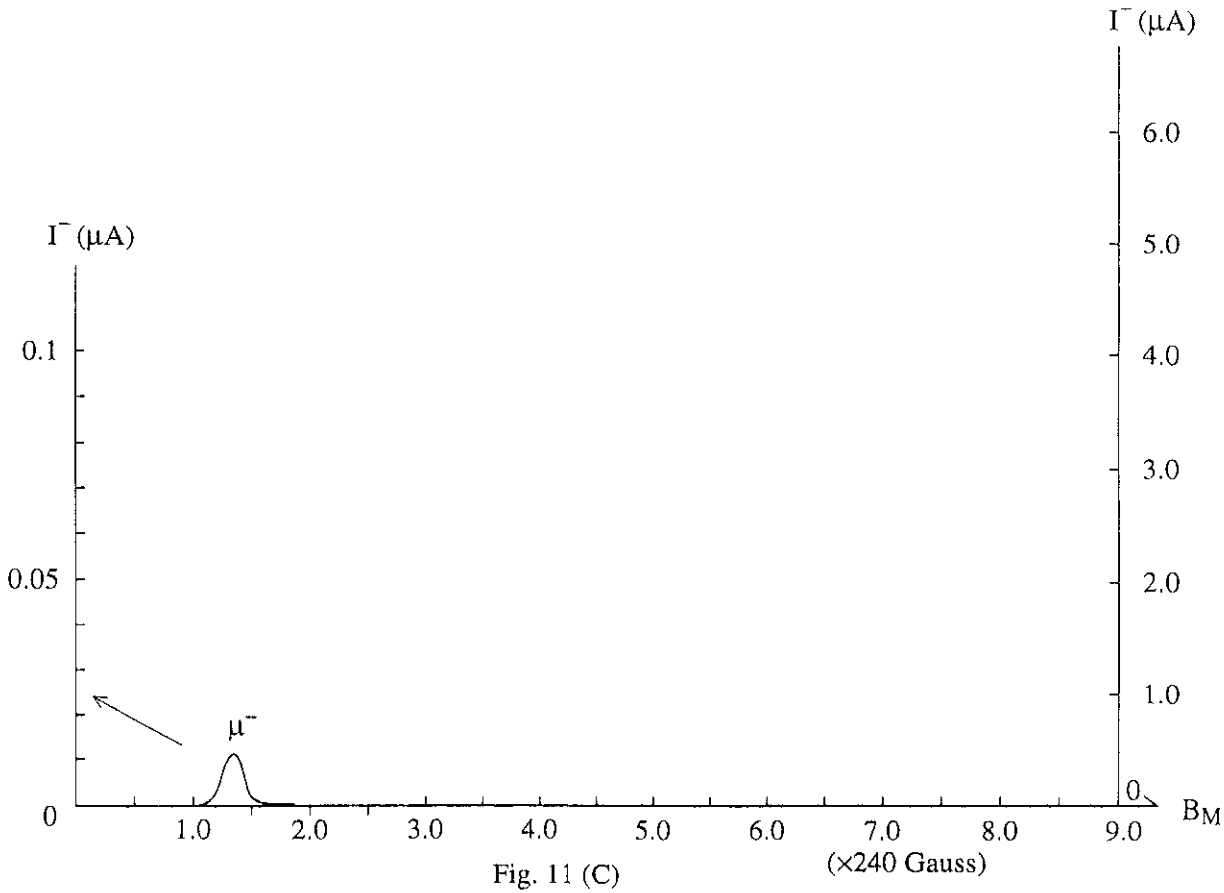

Fig. 11 (C)

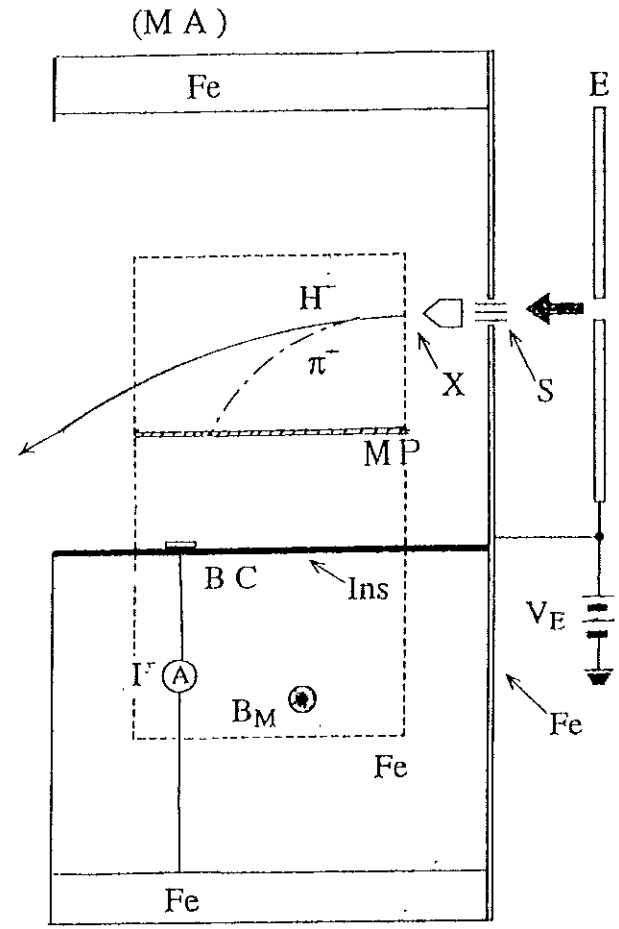

Fig. 12

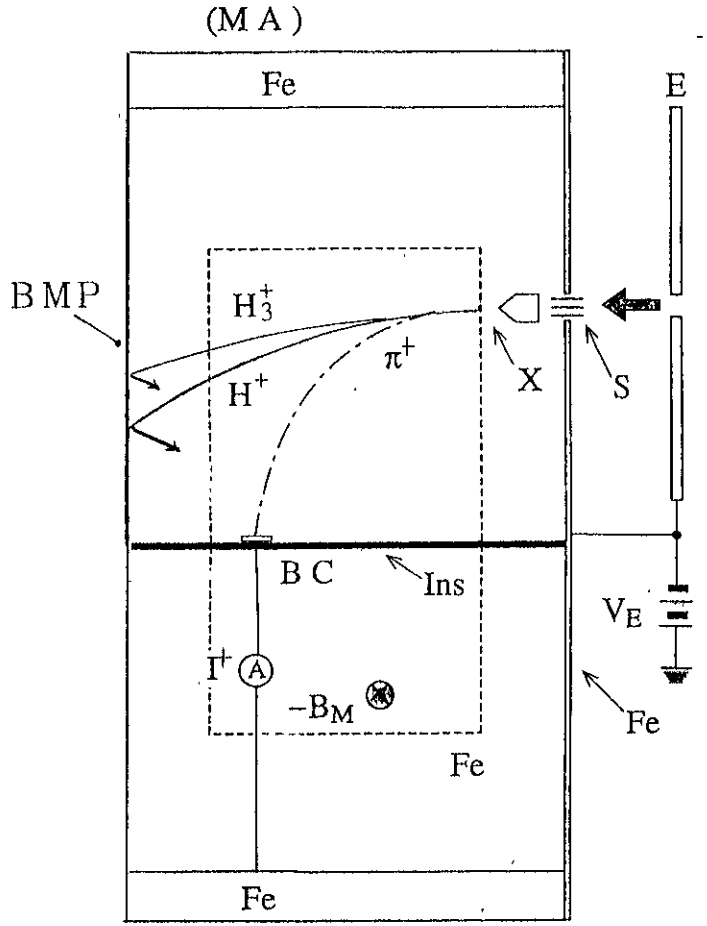

Fig. 13 (A)

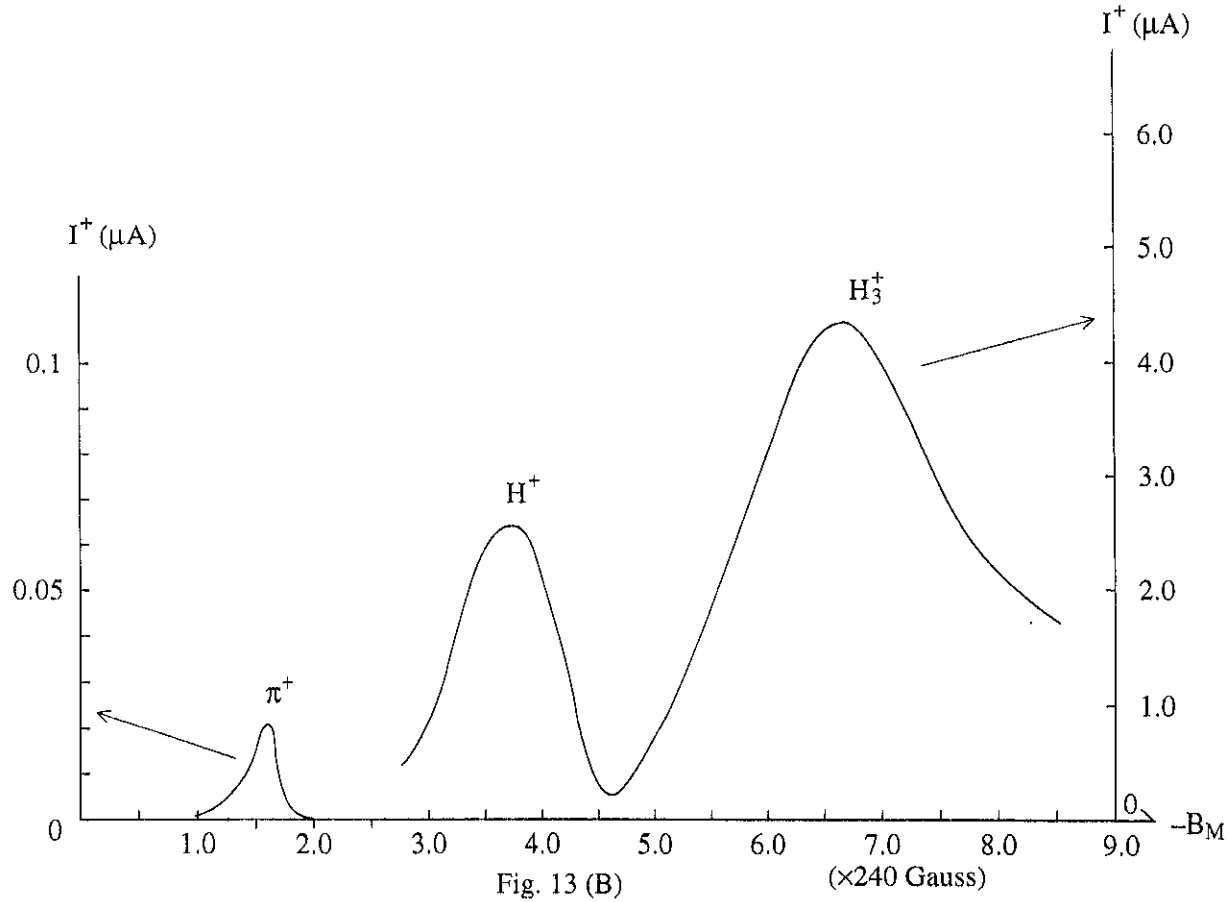

Fig. 13 (B)

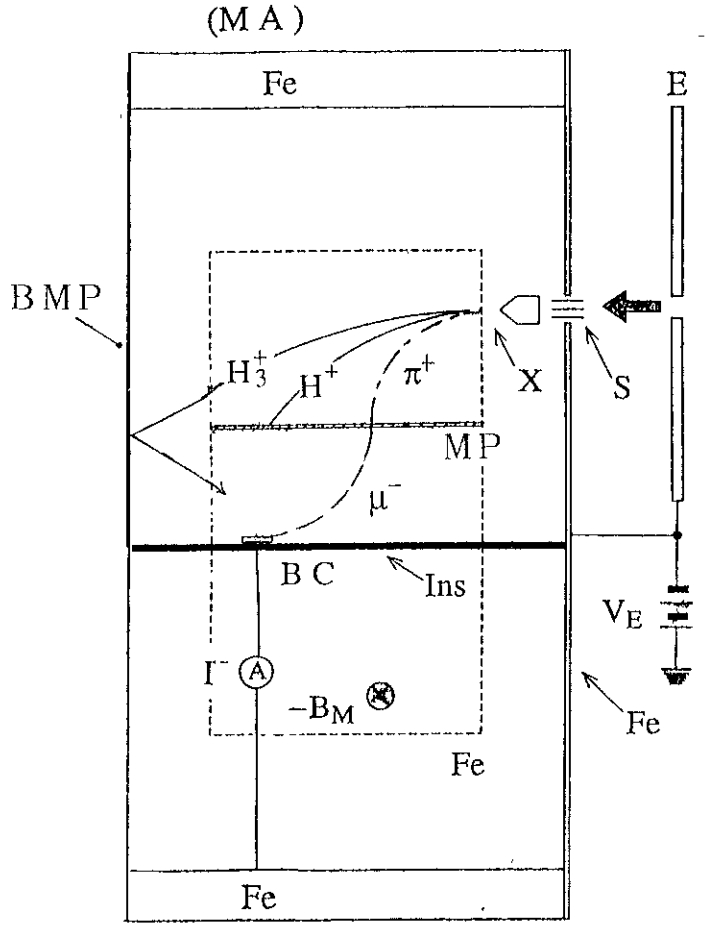

1cm

Fig. 14 (A)

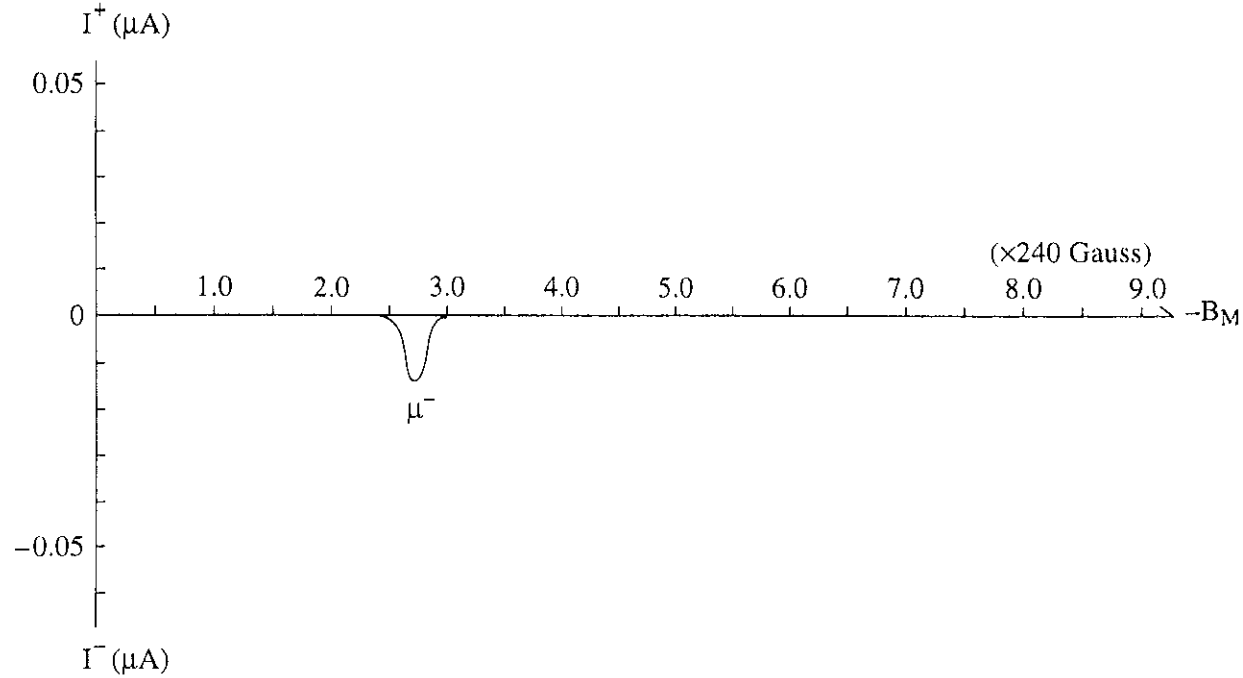

Fig. 14 (B)

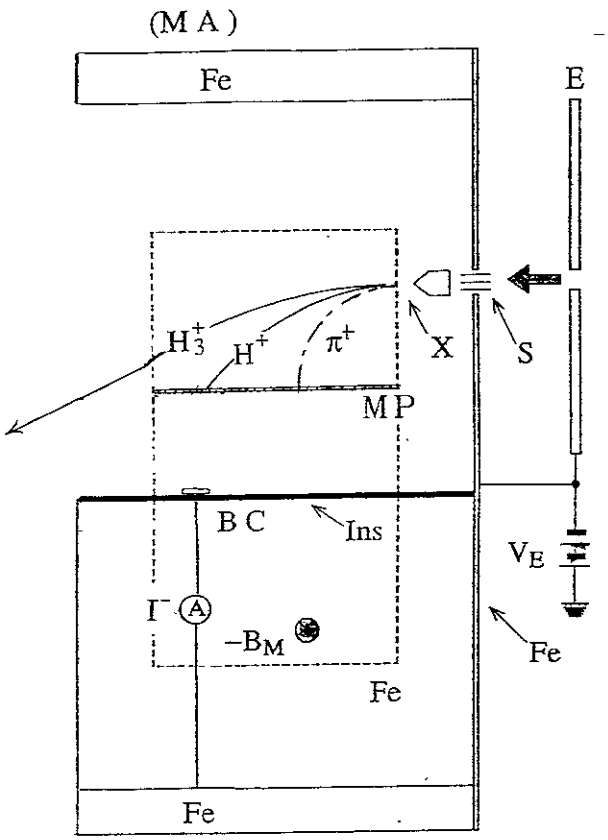

1cm

Fig. 15

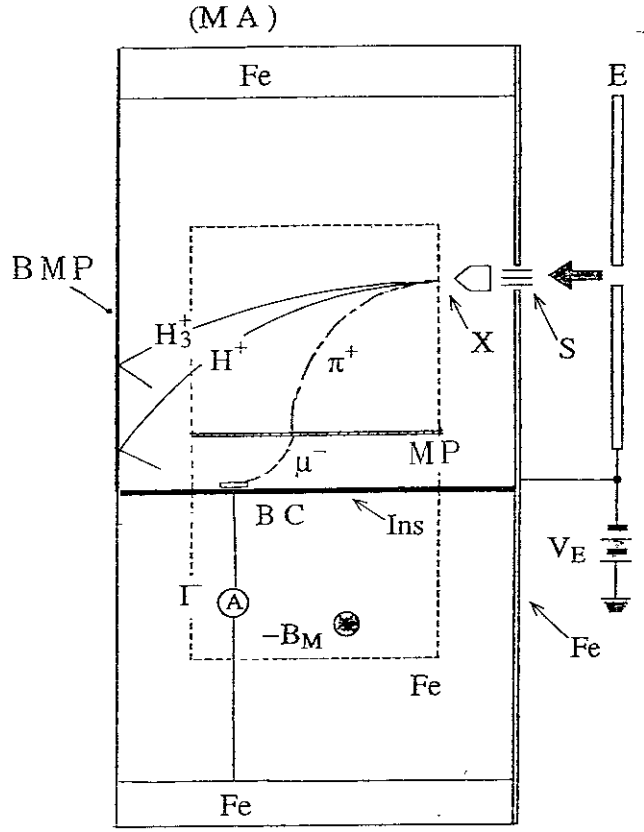

1cm

Fig. 16 (A)

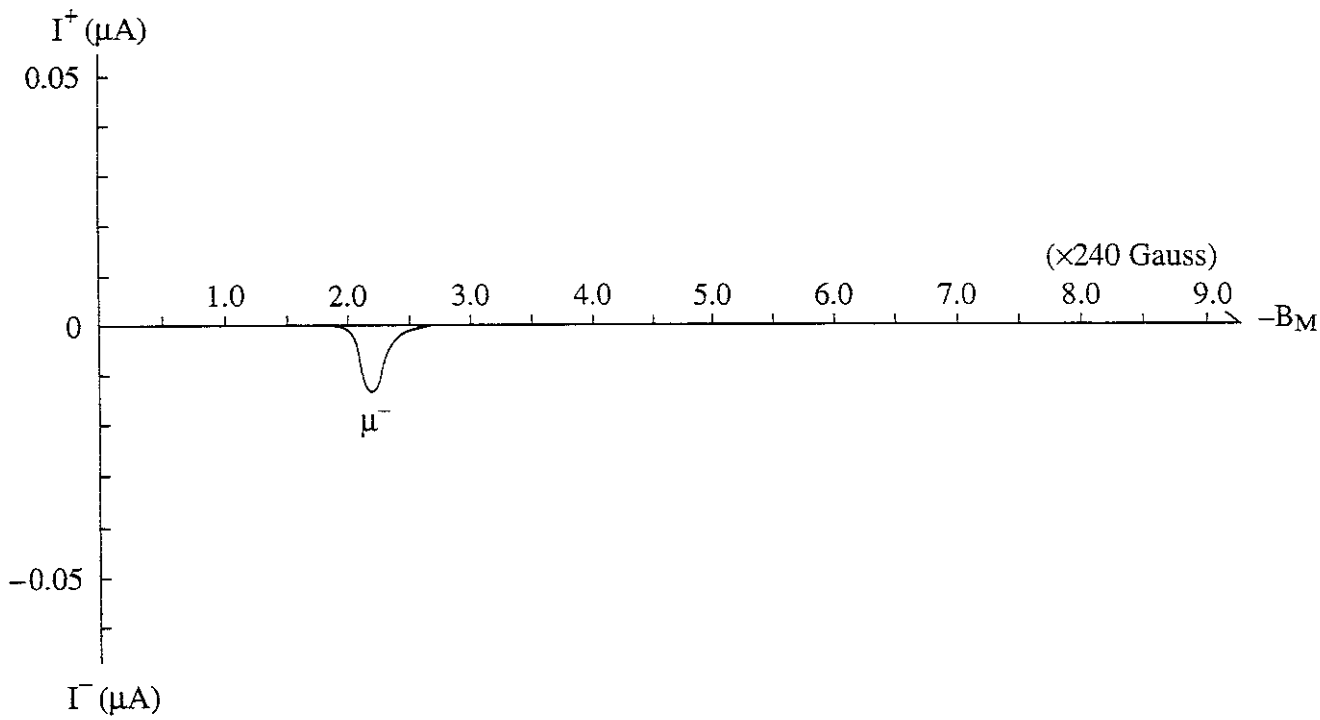

Fig. 16 (B)

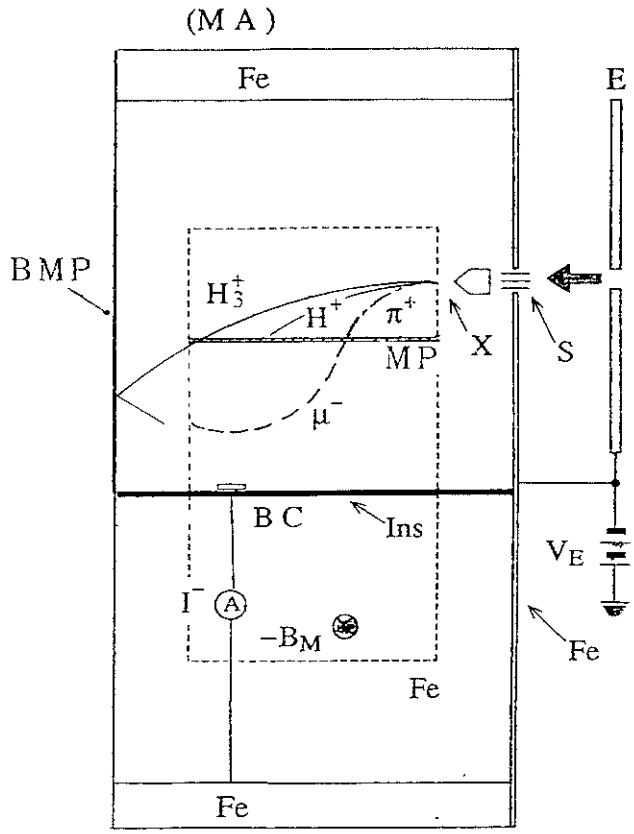

Fig. 17

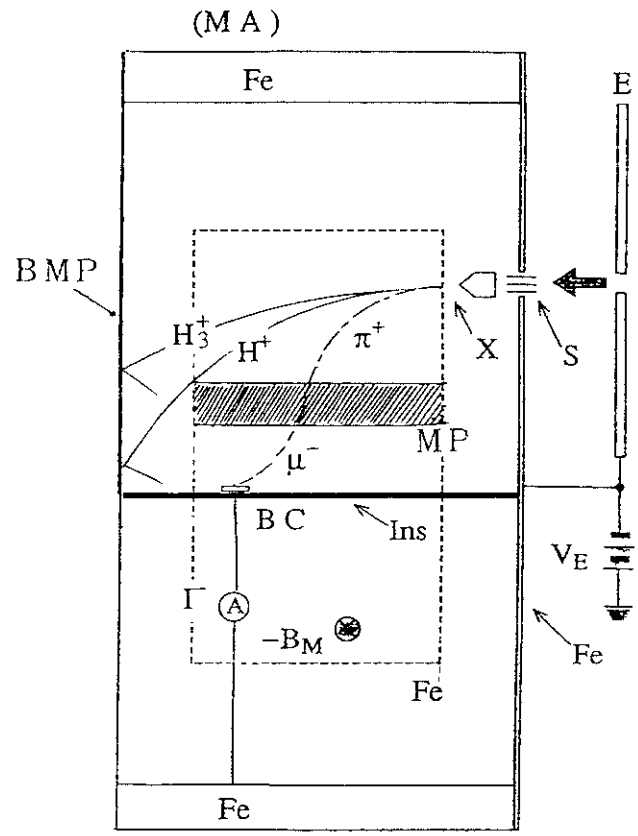

Fig. 18 (A)

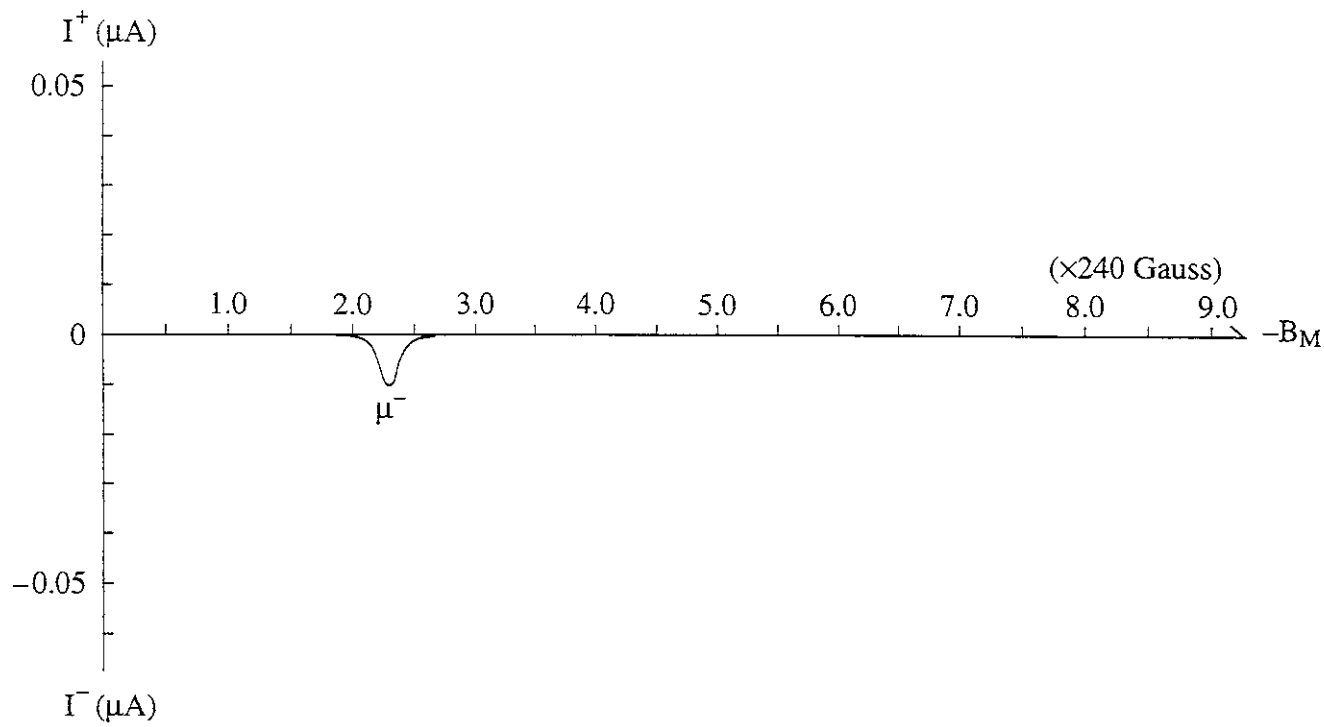

Fig. 18 (B)

Recent Issues of NIFS Series

NIFS-507 R.L Dewar,
Reduced form of MHD Lagrangian for Ballooning Modes, Sep 1997

NIFS-508 Y -N Nejoh,
Dynamics of the Dust Charging on Electrostatic Waves in a Dusty Plasma with Trapped Electrons; Sep.1997

NIFS-509 E Matsunaga, T.Yabe and M. Tajima,
Baroclinic Vortex Generation by a Comet Shoemaker-Levy 9 Impact, Sep. 1997

NIFS-510 C.C Hegna and N. Nakajima,
On the Stability of Mercier and Ballooning Modes in Stellarator Configurations, Oct 1997

NIFS-511 K. Orito and T. Hatori,
Rotation and Oscillation of Nonlinear Dipole Vortex in the Drift-Unstable Plasma; Oct. 1997

NIFS-512 J Uramoto,
Clear Detection of Negative Pionlike Particles from H_2 Gas Discharge in Magnetic Field, Oct 1997

NIFS-513 T. Shimozuma, M. Sato, Y Takita, S Ito, S Kubo, H Idei, K Ohkubo, T Watari, T.S. Chu, K. Felch, P Cahalan and C.M Loring, Jr,
The First Preliminary Experiments on an 84 GHz Gyrotron with a Single-Stage Depressed Collector; Oct. 1997

NIFS-514 T Shimozuma, S. Morimoto, M Sato, Y Takita, S Ito, S. Kubo, H Idei, K Ohkubo and T Watari,
A Forced Gas-Cooled Single-Disk Window Using Silicon Nitride Composite for High Power CW Millimeter Waves, Oct. 1997

NIFS-515 K. Akaishi,
On the Solution of the Outgassing Equation for the Pump-down of an Unbaked Vacuum System; Oct. 1997

NIFS-516 *Papers Presented at the 6th H-mode Workshop (Seeon, Germany)*; Oct 1997

NIFS-517 John L. Johnson,
The Quest for Fusion Energy; Oct 1997

NIFS-518 J Chen, N. Nakajima and M Okamoto,
Shift-and-Inverse Lanczos Algorithm for Ideal MHD Stability Analysis; Nov. 1997

NIFS-519 M. Yokoyama, N. Nakajima and M Okamoto,
Nonlinear Incompressible Poloidal Viscosity in L=2 Heliotron and Quasi-Symmetric Stellarators; Nov. 1997

NIFS-520 S Kida and H. Miura,
Identificaiton and Analysis of Vortical Structures; Nov 1997

NIFS-521 K. Ida, S. Nishimura, T Minami, K. Tanaka, S Okamura, M Osakabe, H. Idei, S Kubo, C Takahashi and K. Matsuoka,
High Ion Temperature Mode in CHS Heliotron/torsatron Plasmas; Nov. 1997

NIFS-522 M. Yokoyama, N. Nakajima and M. Okamoto,
Realization and Classification of Symmetric Stellarator Configurations through Plasma Boundary Modulations, Dec 1997

NIFS-523 H Kitauchi,
Topological Structure of Magnetic Flux Lines Generated by Thermal Convection in a Rotating Spherical Shell; Dec 1997

NIFS-524 T. Ohkawa,
Tunneling Electron Trap, Dec 1997

NIFS-525 K Itoh, S.-I Itoh, M. Yagi, A Fukuyama,
Solitary Radial Electric Field Structure in Tokamak Plasmas, Dec. 1997

NIFS-526 Andrey N. Lyakhov,
Alfven Instabilities in FRC Plasma; Dec. 1997

NIFS-527 J. Uramoto,
Net Current Increment of negative Muonlike Particle Produced by the Electron and Positive Ion Bunch-method; Dec. 1997

NIFS-528 Andrey N. Lyakhov,
Comments on Electrostastic Drift Instabilities in Field Reversed Configuraiton; Dec 1997

NIFS-529 J. Uramoto,
Pair Creation of Negative and Positive Pionlike (Muonlike) Particle by Interaction between an Electron Bunch and a Positive Ion Bunch; Dec. 1997

NIFS-530 J. Uramoto,
Measuring Method of Decay Time of Negative Muonlike Particle by Beam Collector Applied RF Bias Voltage; Dec. 1997

NIFS-531 J. Uramoto,
Confirmation Method for Metal Plate Penetration of Low Energy Negative Pionlike or Muonlike Particle Beam under Positive Ions; Dec. 1997

NIFS-532 J. Uramoto,
Pair Creations of Negative and Positive Pionlike (Muonlike) Particle or K Mesonlike (Muonlike) Particle in H2 or D2 Gas Discharge in Magnetic Field; Dec 1997

NIFS-533 S. Kawata, C. Boonmee, T. Teramoto, L Drska, J Limpouch, R. Liska, M Sinor,
Computer-Assisted Particle-in-Cell Code Development, Dec 1997

NIFS-534 Y. Matsukawa, T. Suda, S. Ohnuki and C. Namba,
Microstructure and Mechanical Property of Neutron Irradiated TiNi Shape Memory Alloy, Jan. 1998

NIFS-535 A Fujisawa, H. Iguchi, H. Idei, S. Kubo, K. Matsuoka, S. Okamura, K. Tanaka, T. Minami, S. Ohdachi, S. Morita, H. Zushi, S. Lee, M. Osakabe, R. Akiyama, Y. Yoshimura, K. Toi, H. Sanuki, K. Itoh. A. Shimizu, S. Takagi, A. Ejiri, C. Takahashi, M. Kojima, S. Hidekuma, K. Ida, S. Nishimura, N. Inoue, R. Sakamoto, S.-I. Itoh, Y. Hamada, M. Fujiwara,
Discovery of Electric Pulsation in a Toroidal Helical Plasma; Jan. 1998

NIFS-536 Lj.R. Hadzievski, M.M. Skoric, M. Kono and T. Sato,
Simulation of Weak and Strong Langmuir Collapse Regimes; Jan. 1998

NIFS-537 H. Sugama, W. Horton,
Nonlinear Electromagnetic Gyrokinetic Equation for Plasmas with Large Mean Flows; Feb. 1998

NIFS-538 H. Iguchi, T.P. Crowley, A. Fujisawa, S. Lee, K. Tanaka, T. Minami, S. Nishimura, K. Ida, R. Akiyama, Y. Hamada, H., Idei. M. Isobe, M. Kojima, S. Kubo, S. Morita, S. Ohdachi, S. Okamura, M. Osakabe, K. Matsuoka, C. Takahashi and K. Toi,
Space Potential Fluctuations during MHD Activities in the Compact Helical System (CHS); Feb. 1998

NIFS-539 Takashi Yabe and Yan Zhang,
Effect of Ambient Gas on Three-Dimensional Breakup in Coronet Formation Process, Feb. 1998

NIFS-540 H. Nakamura, K. Ikeda and S. Yamaguchi,
Transport Coefficients of InSb in a Strong Magnetic Field; Feb. 1998

NIFS-541 J. Uramoto,
Development of ν_μ Beam Detector and Large Area ν_μ Beam Source by H_2 Gas Discharge (I); Mar. 1998

NIFS-542 J. Uramoto,
Development of $\bar{\nu}_\mu$ Beam Detector and Large Area $\bar{\nu}_\mu$ Beam Source by H_2 Gas Discharge (II); Mar. 1998

NIFS-543 J. Uramoto,
Some Problems inside a Mass Analyzer for Pions Extracted from a H_2 Gas Discharge; Mar. 1998